

From skin mechanics to tactile neural coding: Predicting afferent neural dynamics during active touch and perception

Yuyang Wei, Francis P McGlone, Andrew G Marshall, Adarsh Makdani, Zhenmin Zou, Lei Ren* and Guowu Wei*

1
2 **Abstract**— First order cutaneous neurons allow object
3 recognition, texture discrimination, and sensorimotor
4 feedback. Their function is well-investigated under passive
5 stimulation while their role during active touch or
6 sensorimotor control is understudied. To understand how
7 human perception and sensorimotor controlling strategy
8 depend on cutaneous neural signals under active tactile
9 exploration, the finite element (FE) hand and Izhikevich
10 neural dynamic model were combined to predict the
11 cutaneous neural dynamics and the resulting perception
12 during a discrimination test. Using *in-vivo* microneurography
13 generated single afferent recordings, 75% of the data was
14 applied for the model optimization and another 25% was
15 used for validation. By using this integrated numerical model,
16 the predicted tactile neural signals of the single afferent fibers
17 agreed well with the microneurography test results, achieving
18 the out-of-sample values of 0.94 and 0.82 for slowly adapting
19 type I (SAI) and fast adapting type I unit (FAI) respectively.
20 Similar discriminating capability with the human subject was
21 achieved based on this computational model. Comparable
22 performance with the published numerical model on
23 predicting the cutaneous neural response under passive
24 stimuli was also presented, ensuring the potential
25 applicability of this multi-level numerical model in studying
26 the human tactile sensing mechanisms during active touch.
27 The predicted population-level 1st order afferent neural
28 signals under active touch suggest that different coding
29 strategies might be applied to the afferent neural signals
30 elicited from different cutaneous neurons simultaneously.

31
32 **Index Terms**—Neurophysiological, skin mechanics, FE
33 Human hand, neural coding, active touch.

Yuyang Wei is with the Department of Mechanical, Aerospace and Civil Engineering, The University of Manchester, Manchester M13 9PL, UK

Francis P McGlone is with the School of Natural Sciences and Psychology, Liverpool John Moores University, Liverpool L3 5UX, UK

Andrew G Marshall is with the Institute of Aging and Chronic Disease, University of Liverpool, Liverpool, UK and also with the School of Natural Sciences and Psychology, Liverpool John Moores University, Liverpool L3 5UX, UK

Adarsh Makdani is with the School of Natural Sciences and Psychology, Liverpool John Moores University, Liverpool L3 5UX, UK

Zhenmin Zou is with the Department of Mechanical, Aerospace and Civil Engineering, The University of Manchester, Manchester M13 9PL, UK

Lei Ren is with the Department of Mechanical, Aerospace and Civil Engineering, The University of Manchester, Manchester M13 9PL, UK and also with the Key Laboratory of Bionic Engineering, Ministry of Education, Jilin University, China (e-mail: lei.ren@manchester.ac.uk)

Guowu Wei is with the School of Science, Engineering and Environment, University of Salford, Manchester M5 4WT, UK (email: g.wei@salford.ac.uk)

I. INTRODUCTION

34
35 **O**ur ability to perceive and manipulate objects relies
36 fundamentally on subclasses of primary mechanosensory
37 neurons in the glabrous skin of the hand. They provide
38 tactile feedback enabling our somatosensory system to
39 inform the sensorimotor control loop and build the
40 interface between the world and the somatosensory cortex.
41 The closed-loop control allows us to voluntarily perceive
42 and manipulate objects during active touch, acquiring the
43 information based on perception. The typical case of
44 sensorimotor control is the reflex caused between
45 cutaneous mechanoreceptors and the efferent motor neuron
46 modulating muscle forces [1, 2]. The external stimuli are
47 encoded by cutaneous receptors as 1st order afferent neural
48 signals and then transmitted to the spinal cord and higher
49 central nervous system (CNS) for further processing and
50 decoding [3].

51 Over the past decades, research has focused on capturing
52 the single-fiber afferent signals from the peripheral neural
53 system [4, 5] using the technique of microneurography,
54 applying numerical models to understand the neural
55 dynamics and the mechano-electrical mechanisms of the
56 cutaneous receptors under different stimulus conditions.
57 Quantifying the relationships between the stimuli and the
58 state of stress/strain at the site of mechanoreceptors. In
59 2003, Dandekar et al. showed that the strain energy density
60 can be quantitatively related with the membrane current
61 through the cutaneous receptor and then applied this for
62 predicting neural dynamics [6]. Another study was
63 conducted by delivering passive stimuli to the finite
64 element (FE) model, strain energy density (SED) was
65 extracted for evaluating the afferent neural signals and
66 validated against the microneurography results [7]. Similar
67 numerical models based on continuum mechanics have
68 also been applied to simulate population-level afferent
69 signals under passive stimulation using model parameters
70 derived from afferent spiking data in monkey glabrous skin
71 [8]. However, previous numerical models did not
72 incorporate the lateral sliding, realistic skin contact
73 mechanism, or the hyper-elastic material properties of soft
74 tissues. Also, muscle actuated active touch was not
75 integrated with the numerical model, only passive stimuli

76 were simulated with the simplified FE finger-tip model [7,
 77 9]. It has been shown that different skin mechanics and
 78 neural responses during active touch could be altered from
 79 those evoked by passive stimuli [10-12]. However, the
 80 neural dynamics under muscle-driven active touch are
 81 difficult to capture using microneurography since the
 82 subject needs to be restrained and have relaxed muscles
 83 since electromyography signals may mask the afferent
 84 signals [13]. Therefore, the neural response or the
 85 mechano-electrical properties of cutaneous neurons under
 86 active touch still remains unknown [8, 14] warranting
 87 being explicitly studied through the muscle-driven FE hand
 88 model.
 89 Tactile perception is based on the integrated and
 90 processed population-level afferent signals from 1st order
 91 low threshold mechanoreceptors (LTM) in the skin, relays
 92 in the dorsal column nuclei and then via the thalamus to the
 93 somatosensory cortex. Research has shown that the
 94 collection of the group responses from 1st order cutaneous
 95 neurons is critical for understanding the tactile neural
 96 coding and the sensorimotor mechanism [2, 14]. Therefore,
 97 the second step of neural coding after the 1st order
 98 cutaneous mechanoreceptors is to understand how
 99 perception depends on these population-level afferent
 100 dynamics [3], the external stimuli should be related to the
 101 final human percept across the intact afferent transduction
 102 path under the active touch. The relationship between

103 perception and afferent dynamics has been studied using
 104 *in-vivo* neural microstimulation of single peripheral
 105 afferents and the somatosensory cortex in awake subjects.
 106 Electrical stimulation of single afferent fibers in awake
 107 humans through a microneurography recording electrode, a
 108 technique termed intra-neural microstimulation, first
 109 reported by Ochoa et al [15], indicating that activity in a
 110 single afferent fiber could be perceived with perceptual
 111 qualities that depend upon the afferent type. A series of
 112 *in-vivo* tests conducted by stimulating area 3b to study
 113 temporal coding mechanisms in non-human primates [16]
 114 showed that the frequency discrimination of the subjects
 115 may depend on temporal coding and is more general than
 116 rate coding. However, recording afferent dynamics from
 117 population-level afferent fibers is technically demanding,
 118 and the invasive experiment on living subjects cannot be
 119 avoided [17, 18]. Implementation of the numerical model
 120 might be an effective method to obtain the fairly accurate
 121 population-level cutaneous signals and study the coding
 122 mechanism across the intact somatosensory path from the
 123 external stimuli to the final perception. Also, this study
 124 presents the possibility of using FE based integrated
 125 numerical model as a novel method to investigate the
 126 human sensorimotor mechanisms.

128

II. METHODOLOGY

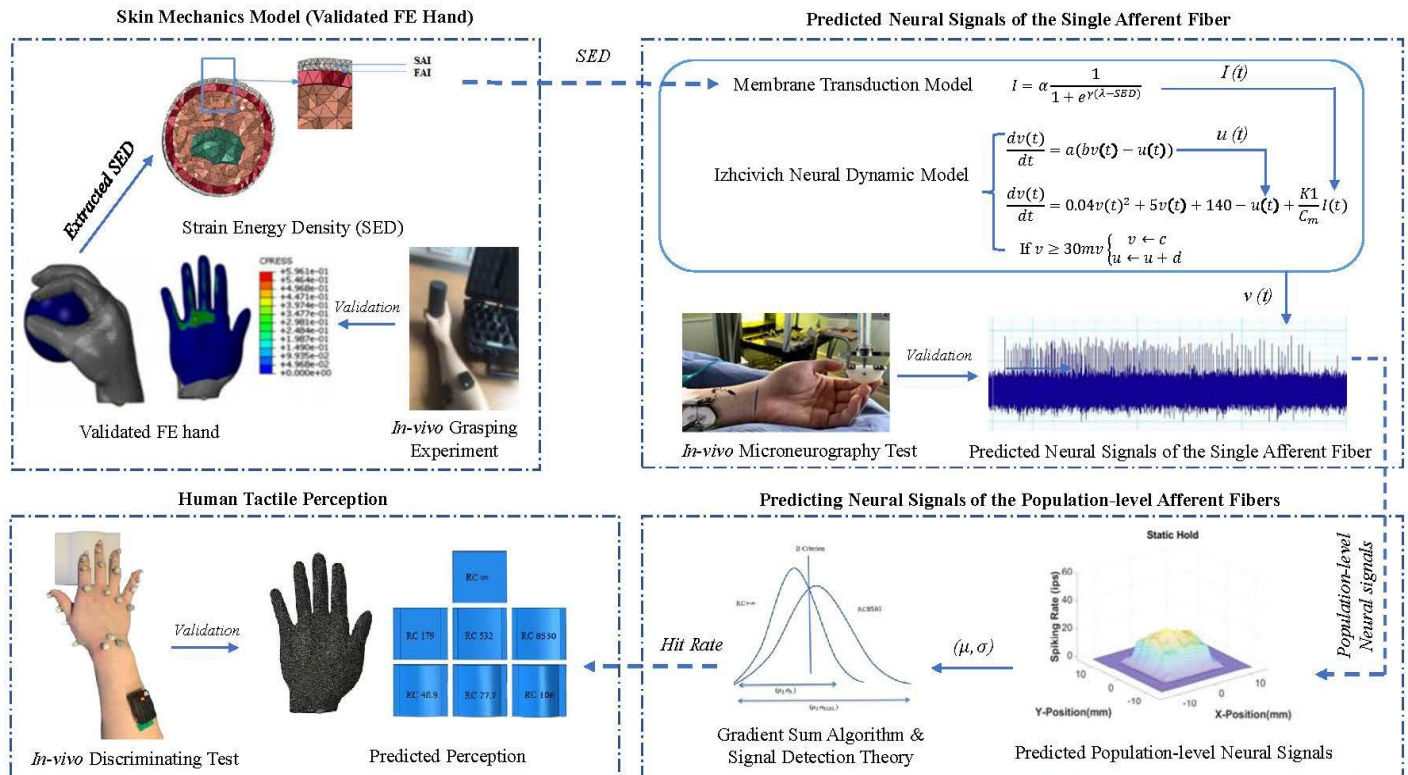


Fig. 1. Main procedure of this research. From the development of the FE human hand model to the predictions of the tactile neural signals. At the first step (Skin mechanics model), the SED during active touch was extracted at the site of mechanoreceptors as input of the membrane transduction model of step 2 (Predicting neural signals of the single afferent fiber). The neural signals from a single afferent tactile fiber were predicted and validated against microneurography results, this procedure was duplicated in step 3 (Predicting neural signals of the population-level afferent fibers) to derive the population-level afferent tactile neural signals. The signal detection theory was employed to correlate the computed neural signals with predicted human perception or the hit rate in step 4 (human tactile perception). The predicted hit rate was validated with the results of the *in-vivo* discrimination test.

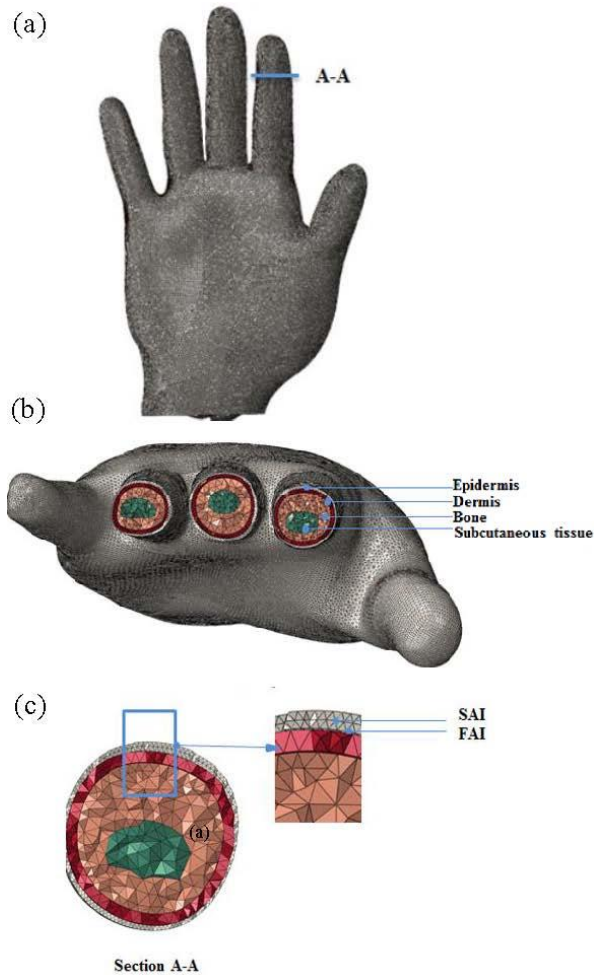


Fig. 2. The skin mechanics model (a). The FE human hand model. (b). The four-layered structure was modelled for extracting proper SED during the active touch including bones, subcutaneous tissue, dermis and epidermis from inside to outside. (c). The cross-sectional view of the index finger. The locations for extracting strain energy density of SAI/FAI mechanoreceptor. The SED of SAI was extracted at the top point of the tetrahedral element at the boundary between the epidermis and dermis while for FAI unit, the SED was computed at the bottom points of the elements on the epidermis-dermis boundary.

129 The integrated numerical model was developed,
 130 optimized and validated on three different levels (see Fig.
 131 1): A) Skin mechanics (strain/stress environment at the site
 132 of the cutaneous mechanoreceptors). B) To give the
 133 explicit transformation between skin mechanics and neural
 134 activity. (Predicted neural action potentials of a signal
 135 tactile fiber were optimized and validated against the
 136 results of microneurography). C) Population-level neural
 137 signals to human perception. (Predicted population-level
 138 tactile neural signals were compared with the *in-vivo*
 139 experimental results, signal detection theory was used to
 140 make the decision). This research began with finding the
 141 parameter to link the skin mechanics with the transduction
 142 membrane current across cutaneous neurons. The SED and
 143 other stress/strain values were compared with the
 144 experimental results of microneurography, and it was
 145 found that SED achieved the most accurate representation
 146 of cutaneous neuron dynamics. The neural signal of a
 147 single tactile afferent fiber was predicted as follows: The
 148 3D FE human hand was used to simulate the procedure of

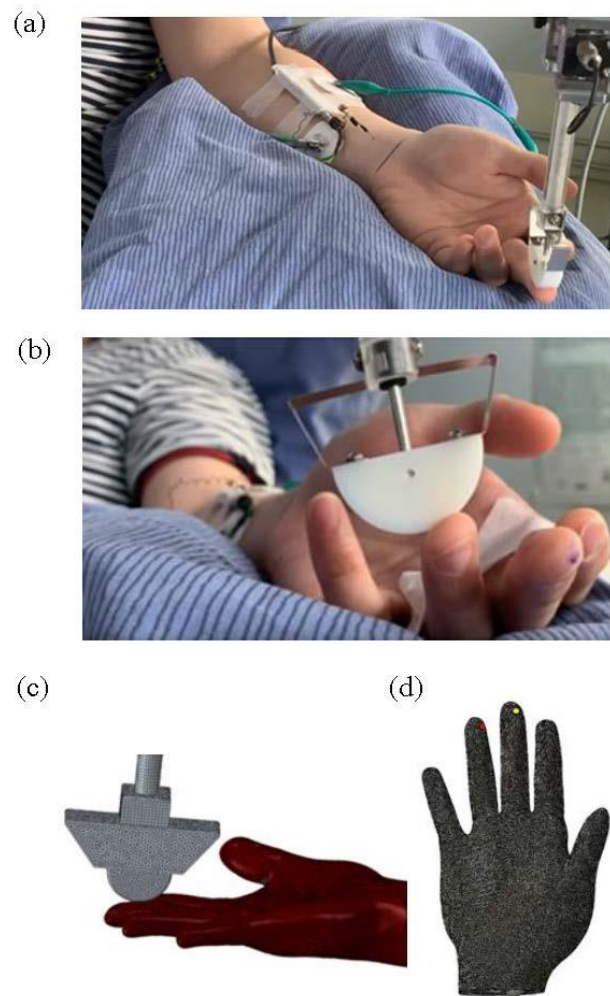


Fig. 3. The Microneurography test and the corresponding FE simulations. (a) Tungsten electrode (FHC Inc. Bowdoin, ME USA) was inserted into median nerve, capturing the single-afferent neural signals. (b). The Robotic Tactile Stimulator (RTS) (Dancer Design Inc. Merseyside, UK) was used to deliver the stimuli onto the receptive field of a tactile unit. The RTS delivered a sweeping motion across the receptive field of the tactile unit with a specified contact force. (c) The FE simulation of the experiment. (d) The locations of the SAI and FAI tactile unit captured during microneurography which are highlighted with yellow and red dot respectively on the FE hand.

149 active touch as skin mechanics model, the SED was chosen
 150 among the stress/strain related values and transferred into
 151 membrane current flowing over the mechanoreceptors by
 152 using the mechano-electrical transduction model. The
 153 Izhikevich neural model was applied to generate the action
 154 potentials based on the predicted membrane current. The
 155 population-level afferent tactile signals were computed
 156 over the fingertips by duplicating the procedure of
 157 converting SED to neural dynamics for the single tactile
 158 afferent fiber. At the same time, the published numerical
 159 model ‘TouchSim’ [8] was employed as the benchmark to
 160 compute neural response under passive stimuli and
 161 compare with the performance of the multi-level numerical
 162 model developed in this research.

163 A. Skin mechanics model-FE human hand

164 A subject-specific FE human hand model [19] (see Fig.
 165 2(a)) was developed to obtain the propagation of
 166 stress/strain during the procedure of active touch. The FE
 167 model includes the geometry of the epidermis, dermis,

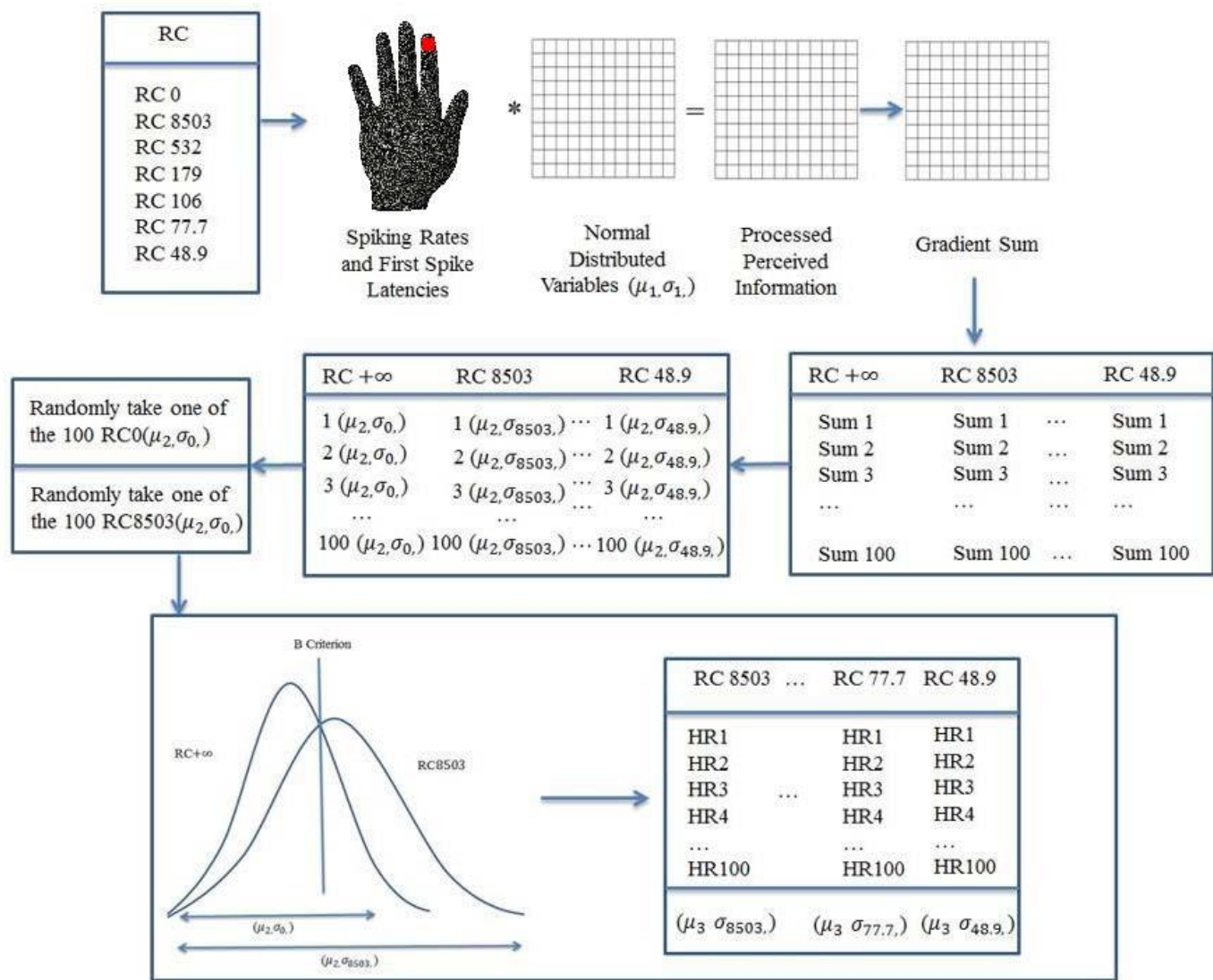


Fig. 4. The flow chart of the gradient sum approach for the population-level validation. Six convex with different radius were discriminated from the flat plate. First, the random noise is added through multiplying the neural action potential or the first spike latency of the tactile units by a pair of random variables with a mean value $\mu=1$ and the standard deviation σ varied between 0.015 and 0.085. Second, the gradient sum of the elements is calculated by summing the gradients of all 100 elements together (100 SAI mechanoreceptors (elements) distributing over 1cm^2 area on the finger pad). Third, the first and second steps are repeated 100 times for all the 6 convex resulting in 600 gradient sums totally, 100 pairs of μ_2, σ_2 are derived for each convex. Fourthly, two pairs of (μ_2, σ_2) from the plate and convex were randomly selected. The signal detection theory (SDT) was used to judge whether the FE hand can differentiate the convex from the flat plate. This procedure is repeated for 100 times and the 100 discrimination accuracies or hit rates (HR) were computed for discriminating each convex surface.

168 subcutaneous tissue (see Fig. 2(b)), and the bones
 169 reconstructed based on the MR and CT images taken from
 170 a 23-year-old male subject. The material properties of soft
 171 tissues were defined as isotropic hyper-elastic, and the
 172 bones were assigned with the isotropic linear elastic
 173 material.

174 The mesh size of the epidermis and dermis was set to be
 175 0.1mm, 0.7mm-mesh size was assigned for subcutaneous
 176 tissue and the bones. 1,002,915 C3D8H elements were
 177 meshed onto this FE hand model. Three grasping (cylinder
 178 grasping, spherical grasping, and precision gripping) were
 179 performed. The predicted results agreed well with the
 180 *in-vivo* experiment in terms of contact pressure and contact
 181 area and the relative differences between the two results are
 182 below 20%. The predicted contact area and contact
 183 pressure can provide the bulk mechanical response of the
 184 tissue layers [19, 20]. The detailed process for developing

185 and validating the FE human hand can be found in our
 186 previous study [19]. Therefore, this FE human hand model
 187 is employed to produce the stress/strain related quantities
 188 as the skin mechanics model.

189 B. Predicting tactile signals of the single afferent neural 190 fiber

191 1) The combined transduction and neural dynamic model 192 for predicting cutaneous neural signals

193 The mechano-electrical transduction function was firstly
 194 applied on the hair cell to explain the transducer adapting
 195 property [21]. Researchers also used these transduction
 196 functions to describe the mechano-electrical transaction
 197 properties of the cutaneous mechanoreceptors and gained a
 198 good accuracy [7, 9, 22]. The SED at the site of the
 199 mechanoreceptor (see Fig. 2(c)) was extracted from the FE
 200 human hand and transformed to membrane current using
 201 the transduction function (equation 1). α, γ, λ are the

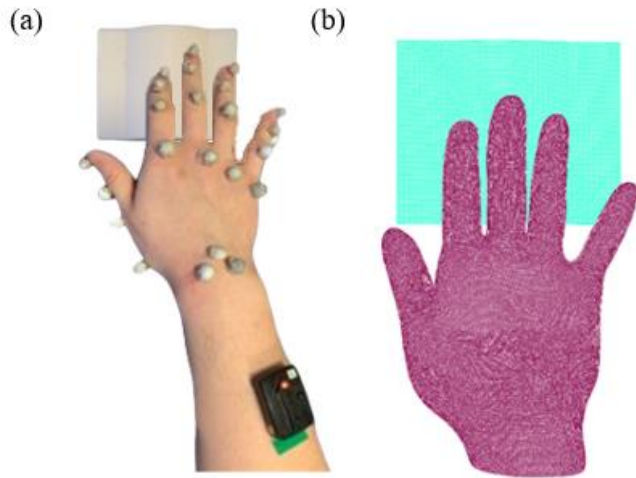


Fig. 5. *In-vivo* differentiation test and the corresponding simulation with the FE human hand (a). The *in-vivo* discrimination test. The subject was blind-folded and asked to differentiate two convex with different radius only through tactile perception. The markers were used to capture the hand kinematics during active touch using the Vicon System (Oxford Metrics Ltd., Bilston, UK). The Delsys Trigno (Delsys Inc., Boston, US) was applied to record EMG signal of the muscle. (b) The FE simulation of the discrimination test.

parameters determined through model fitting when the difference between predicted values and results of microneurography test are minimized.

$$I(SED) = \alpha \frac{1}{1 + e^{\gamma(\lambda - SED)}} \dots \dots \dots (1)$$

The cutaneous LTMs found in the glabrous skin of the human hand have distal axons that branch in the skin with irregularly spaced transduction sites [23, 24]. The spatially complex and overlapped receptive fields of the cutaneous neurons and the distance between the interdigitating subfields might determine the limit of the spatial resolution of human [25]. For this multi-level numerical model, each cutaneous tactile neuron is assumed to branch into 16 sensory organs according to the literature [26-30], echoing the fact that the first-order tactile neurons innervate on the order of ten mechanoreceptors. To simulate the heterogeneous receptive fields with highly sensitive zones of the branched axons, the SED was randomly selected at the nodes in the circular area with a diameter of 3mm [31]. At the same time, the SED was also extracted from the evenly distributed nodes for comparison and evaluating the effects of the non-uniformly distributed receptive fields of cutaneous neurons on tactile performance as is shown in Fig. S1. The neural responses were then computed based on the SED extracted from these nodes under the two different distribution patterns.

To mimic the biological neural dynamics of the tactile mechanoreceptor, the Izhikevich neural dynamic model was applied [32]. This neural dynamic model has been found to be able to reproduce the spiking, bursting response and the adaptation properties of the cutaneous mechanoreceptors [9, 22]. Among the four major types of low-threshold mechanoreceptors in the human hand, the SAI and FAI units were modelled to investigate the human sensing mechanism during spatial discrimination or active exploration in this study. Because the responses of SAI and FAI are critical to detailed feature discrimination [30, 33,

34] and sensorimotor control [35] which enables the explorative role of the hand. The responses of SAI and FAI units play a minor role in feature discrimination [34] which were not included in this numerical model.

The dynamic of the membrane potentials of SAI and FAI are defined as follows:

$$SAI: \frac{dv(t)}{dt} = 0.04v(t)^2 + 5v(t) + 140 - u(t) + \frac{K1}{Cm} I(t) \dots \dots \dots (2)$$

$$\frac{du(t)}{dt} = a(bv(t) - u(t)) \dots \dots \dots (3)$$

$$FAI: \frac{dv(t)}{dt} = 0.04v(t)^2 + 5v(t) + 140 - u(t) + \frac{K2}{Cm} \frac{dl(t)}{dt} \dots \dots \dots (4)$$

$$\frac{du(t)}{dt} = a(bv(t) - u(t)) \dots \dots \dots (5)$$

The auxiliary function is defined as followed:

$$\text{If } v \geq 30mv \begin{cases} v \leftarrow c \\ u \leftarrow u + d \end{cases} \dots \dots \dots (6)$$

Where a,b,c,d are neuron parameters, u is the membrane recovery variable, v is the membrane potential.

2) *In-vivo microneurography test*

The subject gave informed consent to participate in the microneurography recording, which was approved by the Liverpool John Moores University Research Ethics Committee.

To optimize and validate the predicted afferent neural signals, microneurography was carried out. We have found that the spiking features and the selective response property of the same type of tactile units located at fingertips are similar to each other according to our microneurography results and the literature [36-38]. Therefore, the response of a single SAI/FAI tactile unit was recorded and used for developing the integrated numerical model. The same subject involved in developing the FE hand was recruited again for microneurography. The subject was required to lie on a medical chair with the forearm restrained. A tungsten microelectrode (FHC Inc. Bowdoin, US) was inserted into the skin at the wrist and electrical stimulation was delivered through the electrode to roughly determine its position in relation to the median nerve (see Fig. 3(a)). After locating and entering the nerve, the electrode was adjusted manually to search for tactile units. The action potentials were amplified and visualized by Neuro Amp EX and physiological data analysis software LabChart (ADInstruments Ltd. Oxford, UK) respectively. The receptive field was stimulated by the rotatory tactile stimulator (RTS) (Dancer Design Inc. Merseyside, UK) with varying forces (ranging from 0.2 to 2.4N with an increment of 0.2N). The stimulator delivered a ‘sweep’ stimulus onto the marked receptive field of the afferent tactile fiber as are shown in Figure 3(b) and the corresponding FE simulation is presented in Figure 3(c). The locations of the SAI (yellow dot) and FAI (red dot) tactile units captured during microneurography are shown in Figure 3(d). The spiking rates were derived for each second, resulting in 121 data points for the SAI unit under five stimulating forces (0.6, 1.0, 1.4, 1.8, 2.4N) while 131 data points were obtained for the FAI unit under six stimulating forces (0.4, 0.8, 1.2, 1.6, 2.0, 2.4N). The firing rate was calculated by taking the average of the reciprocal inter-spike intervals (ISI):

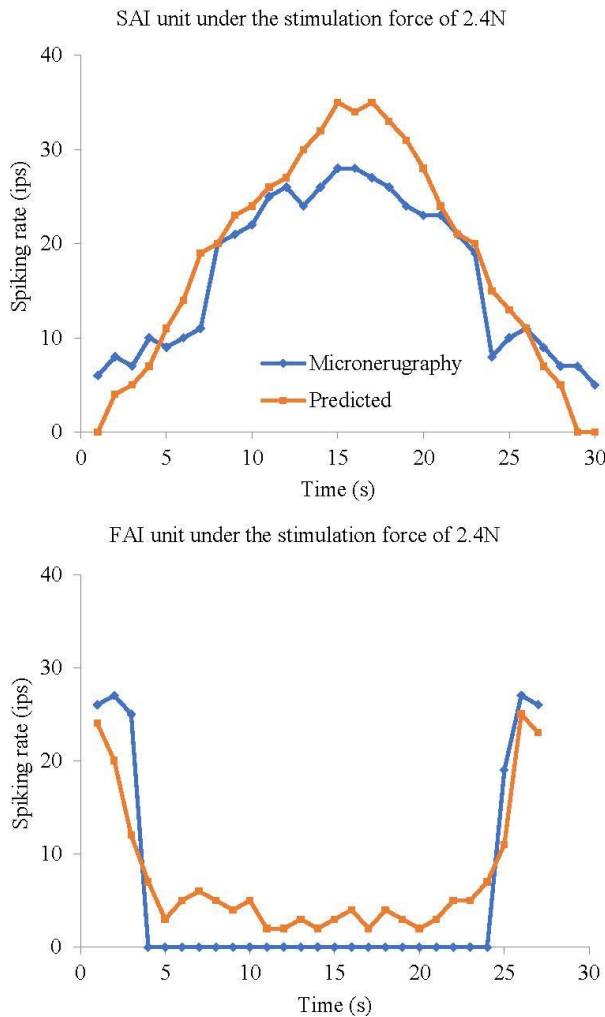


Fig. 6. The validation results for the single SAI and FAI tactile fiber. The predicted neural signals of SAI and FAI unit were compared with the results of microneurography.

295
$$ISI_i = t_i - t_{i-1} \dots \dots \dots (7)$$

296
$$ISI_i = \frac{1}{a-b} \sum_{i=b}^a ISI_i \dots \dots \dots (8)$$

297
$$f = \frac{1}{ISI_d} \dots \dots \dots (9)$$

298 Where a-b= the number of ISIs.

299 3) *Parameter optimization and validation for*
 300 *transduction and neural dynamic model based on the*
 301 *subject-specific microneurography data*

302 The membrane current transduction and neural dynamic
 303 model were optimized against the results of the
 304 microneurography data by using the response surface
 305 method (RSM). Seven parameters in this integrated model
 306 were optimized against experimental results. Similar cross
 307 validation algorithm has been applied by other researchers
 308 to fit the parameters of neural dynamic model with
 309 experimental results [7].

310 The action potential signals under the stimulating force
 311 of 2.4N for SAI and FAI unit were separated for the
 312 validation (out-of-sample validation) while the rest of the
 313 data (Stimulating forces of 0.6, 1.0, 1.4 and 1.8N for SAI
 314 and 0.4, 0.8, 1.2, 1.6, 2.0 for FAI unit) were used to fit the
 315 computational model by using the RSM algorithm. The
 316 seven parameters: α , γ , λ of the transduction model and a, b,

317 c, d of the Izhikevich model were optimized. The RSM
 318 algorithm aims to derive the specific combinations of these
 319 parameters which produce the best goodness of fit. (The
 320 fractional sum of squares (FSS, see equation 10.) between
 321 our subject-specific microneurography data and the
 322 predictions were minimized).

323
$$FSS = 1 - \frac{\sum_{i=1}^n [(exp)_i - (pre)_i]^2}{\sum_{i=1}^n (exp)_i^2} \dots \dots \dots (10)$$

324 Where the *exp* stands for the microneurography test result,
 325 *pre* is the predictive result, n is the number of the data
 326 points.

327 The initial parameters values are $\alpha = 2.46 \times$
 328 10^{-5} mA , $\gamma = 0.0046 \text{ Pa}^{-1}$, $\lambda = 506.74 \text{ Pa}$, a = 0.02
 329 Ohm, b = 0.2, c = -65mv, d = 6mv, these values are
 330 obtained from the literature [9, 39]. The procedure of
 331 parameter optimization was carried out in 4 steps. (a)
 332 Firstly, all the seven parameters were coded with specific
 333 increments less than two orders of magnitude of the initial
 334 values. (b) Secondly, all the parameters were increased or
 335 decreased for one increment and the FSS was derived for
 336 each trial resulting in totally 2^7 combinations. (c) Thirdly,
 337 the relationship between the optimized parameters and the
 338 FSSs was obtained through linear regression. (d) Fourthly,
 339 the magnitude and direction in which to optimize the
 340 parameters were determined by the combinations of the
 341 variation resulting in the largest increment of FSS. (e) Step
 342 (d) was repeated several times until the FSS was no longer
 343 increased. This optimizing procedure was conducted in
 344 Design Expert (Stat-Ease, Inc. US). After optimizing the
 345 parameters by using the RSM algorithm, the predicted
 346 neural signals of the integrated model achieved a good
 347 agreement with the results of microneurography in this
 348 study.

349 C. *Predicting tactile signals of the population-level*
 350 *afferent neural fiber and its perception*

351 1) *The gradient sum algorithm and signal detection*
 352 *theory for relating the population-level neural activities*
 353 *with human perception*

354 The psychophysical prediction is made by simulating the
 355 procedure of active touch during the discrimination test.
 356 The active touch was divided into two different
 357 procedures: 'dynamic ramp-up' and 'static hold', the
 358 former stands for the onset of the contact with an increased
 359 fingertip contact force and the latter represents the
 360 procedure of the stable contact with the object. The FE
 361 hand model was configured in a population density of 100
 362 and 144 receptors/ cm^2 for SAI and FAI units within the
 363 contact area of 1 cm^2 on the fingertip, discriminating the
 364 convex surfaces with different radius of curvature (RC)
 365 ranging from RC8530mm to RC48.9mm. Active touch was
 366 simulated by using the FE hand with the muscle forces and
 367 kinematics captured during the in-vivo discriminating
 368 experiment. The neural activities of the afferent tactile
 369 fibers within the contact area were computed and the
 370 Gradient Sum method [7] was used to correlate the FE
 371 hand's population-level neural dynamic signals with the
 372 discrimination accuracy or the tactile perception. The
 373 Gradient Sum method transmits the parameters between
 374 receptors and derives the gradients of spiking rates or first

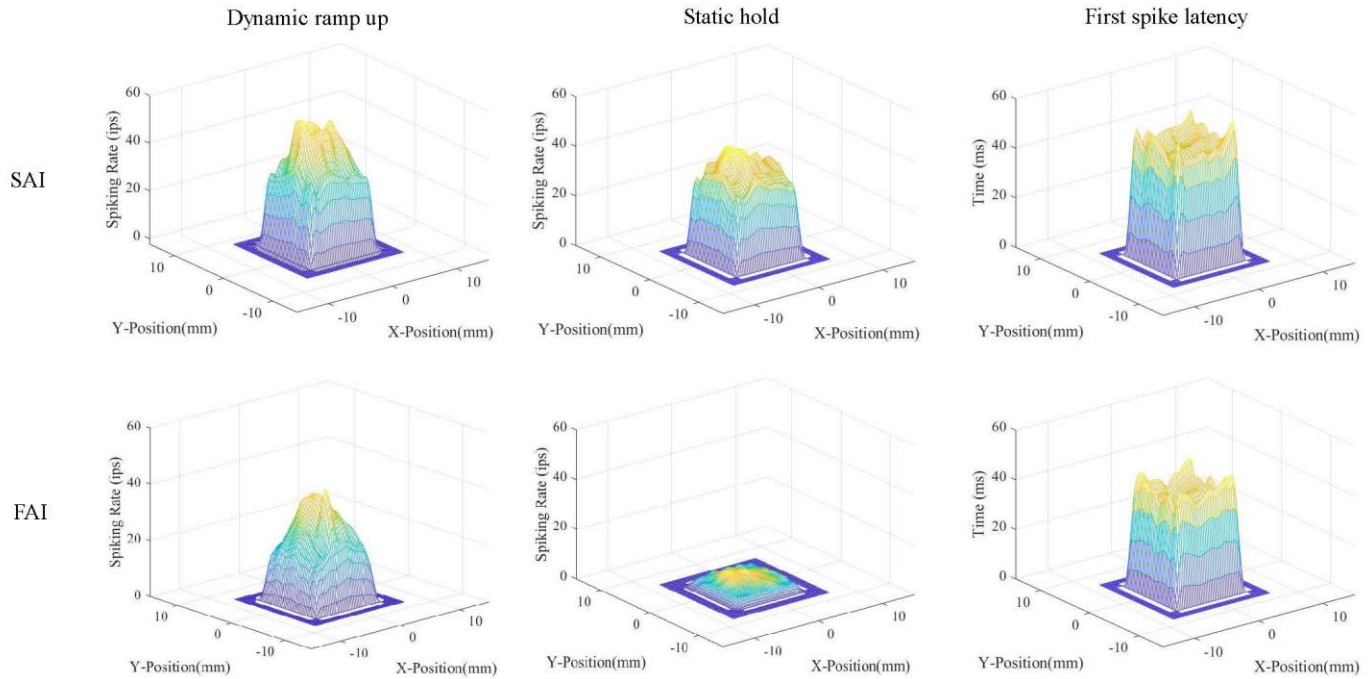


Fig. 7. Predicted neural activities of population-level SAI (first row) and FAI (second row) tactile units on index fingertip under the contact with the convex surface of RC77.7 mm. The horizontal axis stands for the locations of mechanoreceptors within the areas for extracting the SED, the vertical axis is the spiking rate or first spike latency. The active touch was divided into two separate stages including the ‘dynamic ramp-up’ and ‘static hold’.

375 spike latencies from adjacent elements. The procedure of
 376 predicting the population-level tactile neural spike is
 377 shown in Figure 4(a) First, random noises were added
 378 through multiplying neural action potential and first spike
 379 latency of all units in one convex surface by a pair of
 380 random variables (μ_1, σ_1) with mean value $\mu_1=1$ and the
 381 standard deviation σ varied between 0.015 and 0.085. (b)
 382 Second, the gradient sum of the elements is calculated by
 383 summing all the parameter gradients around one single
 384 element. 100 gradients were derived per convex surface
 385 since 100 SAI mechanoreceptors (element) distributing
 386 over 1 cm^2 area was configured for each finger. All the
 387 gradients were added as the gradient sum. (c) Third, steps
 388 (a) to (b) are repeated 100 times for all the 7 convex
 389 surfaces resulting in 700 gradient sums totally, each time
 390 multiplying a new pair of (μ_1, σ_1). The corresponding 100
 391 pairs of (μ_2, σ_2) are derived for each convex. (d) The signal
 392 detection theory (SDT) was used to judge whether the FE
 393 hand can differentiate the convex surface from the flat plate.
 394 For example, two pairs of (μ_2, σ_2) are randomly selected
 395 from RC8503mm convex surface and the flat plate as the
 396 inputs to SDT with the $\beta=0.5$. Therefore, the hit rate (HR)
 397 of convex surface RC8503mm is obtained. This procedure
 398 is repeated for 100 times to derive the 100 HR for
 399 discriminating convex surface RC8503mm. The hit rates
 400 were calculated as below:

$$401 \quad d' = \frac{\mu_s - \mu_n}{\sigma} \dots \dots \dots (11)$$

$$402 \quad d' = \Phi^{-1}(H) - \Phi^{-1}(F) \dots \dots \dots (12)$$

$$403 \quad \ln(\beta) = \frac{[\Phi^{-1}(F)]^2 - [\Phi^{-1}(H)]^2}{2} \dots \dots \dots (13)$$

404 d' is the distance between the means of the signal and noise
 405 in standard deviation units. μ_s and μ_n are the mean values

406 of the signal and noise, σ stands for the standard deviation
 407 of the noise. β is the criterion value and Φ^{-1} is the inverse
 408 ‘Phi’ function of the Z distribution, the detailed
 409 information and calculation related to SDT can be found in
 410 [40].

411 (e) Finally, the step (d) is repeated for the other 5 convex
 412 surface and generates 500 HR. The (μ_3, σ_3) for each 100
 413 HR of all the 6 convex surfaces are calculated. The
 414 procedure of predicting population-level neural signals of
 415 FAI units is the same with SAI.

416
 417 2) *In-vivo discrimination test*

418 A psychophysical test of convex surface differentiation
 419 was performed to validate the predicted population-level
 420 afferent signals and study the neural coding mechanisms
 421 under the active touch. The *in-vivo* discrimination test was
 422 performed based on Goodwin’s research to determine the
 423 discrimination ability of humans [41].

424 To perform the discrimination test of population-level
 425 validation of SAI afferents, six convex surfaces with radius
 426 of RC8503, RC532, RC179, RC106, RC77.7, RC48.9mm
 427 and a flat plate ($RC\infty$) were 3D printed. The same subject
 428 of the FE human hand model was recruited for the
 429 discrimination test. The capability of the subject to
 430 discriminate surfaces during the procedure of active touch
 431 was evaluated with 6 comparisons between different
 432 convex surfaces and the flat plates conducted. The subject
 433 was blindfolded and asked to sit at a table where the convex
 434 surfaces were presented in pairs, either with the same or
 435 different radius. The subject was required to judge whether
 436 the convex surfaces were the same or not. Only the
 437 fingertip of the index was allowed to touch the convex

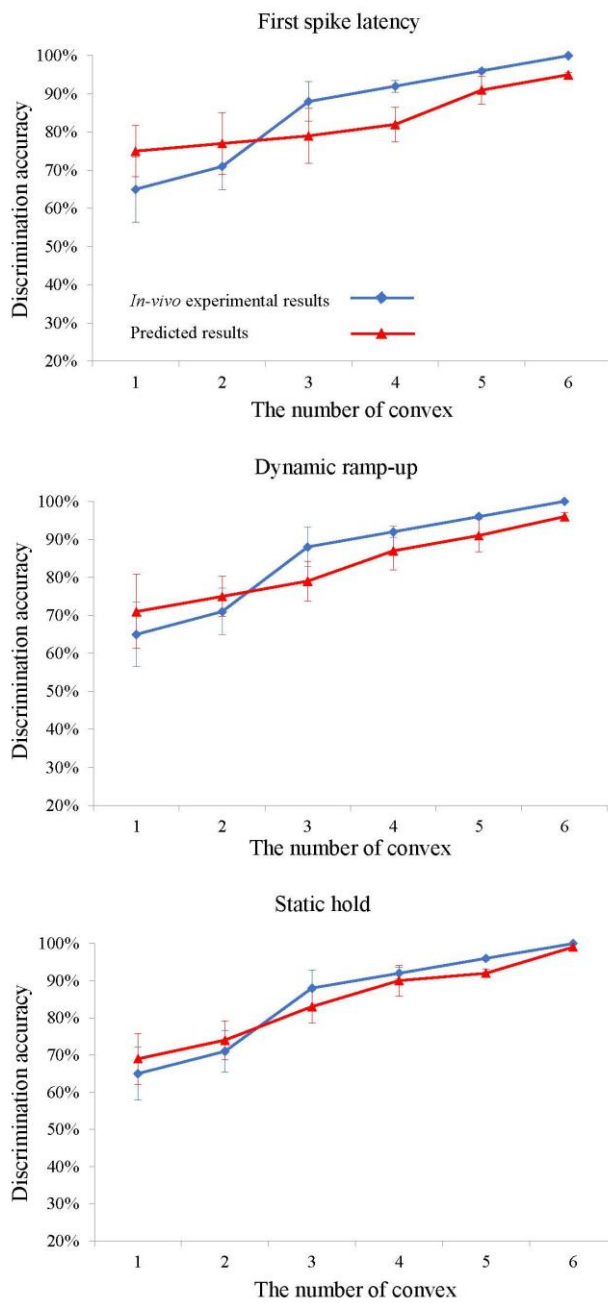


Fig. 8. The validation results of the population-level SAI tactile fibers. The predicted discrimination accuracy based on the afferent neural signals of SAI units were compared with the results of the *in-vivo* discrimination experiment.

438 surfaces and the finger was restricted from
 439 adduction/abduction. The vertical distance between the
 440 peak of the convex surfaces and the index fingertip was
 441 kept the same, ensuring similar finger kinematics during
 442 touching different convex to avoid the effect of the
 443 proprioceptors located at finger joints. The test was carried
 444 out in blocks, each block contained 12 comparisons (6 pairs
 445 of flat-flat plate and 6 pairs of flat-convex, all convex
 446 surfaces were presented in each session), and the pair of
 447 surfaces varied randomly from block to block. In total, 30
 448 blocks were performed, and the probability of detection
 449 was calculated for each convex surface, the whole test was
 450 repeated 6 times to achieve generality. Before the test, a
 451 few practice blocks were performed to train the subjects

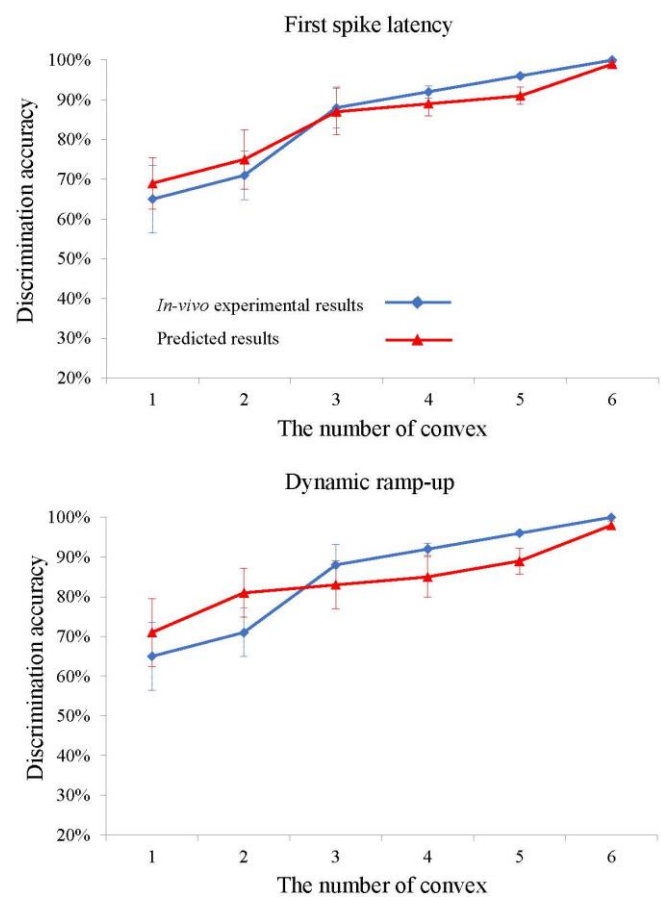


Fig. 9. The validation results of the population-level FAI tactile fibers. The predicted discrimination accuracy based on the afferent neural signals of FAI units were compared with the results of the *in-vivo* discrimination experiment.

452 and ensure the reliability of the experimental results.
 453 During the discrimination test, the hand kinematics and
 454 muscle forces were captured by using the Vicon system
 455 (Oxford Metrics Ltd., Bilston, UK) and Delsys EMG
 456 Trigno (Delsys Inc., Boston, US) respectively (see Fig.
 457 5(a)). The muscle forces were estimated based on the
 458 electromyography (EMG) signals. Before the
 459 discrimination test, maximum voluntary contraction (MVC)
 460 tests were carried out for each muscle using a Jamar
 461 dynamometer. The recorded EMG data was band-pass
 462 filtered (20–400 Hz) with a Butterworth filter and then
 463 rectified. The muscle forces were computed based on the
 464 maximum voluntary contraction forces. It was assumed
 465 that a linear relationship between the EMG signal and
 466 muscle force for isometric muscle contracting. Similar
 467 methods have been used by other researchers to calculate
 468 muscle forces under isometric contract [42–44]. These
 469 kinematic data and muscle forces were applied onto the FE
 470 human hand to simulate the discriminating experiment and
 471 then made the prediction (see Fig. 5(b)). The active touch
 472 procedure was divided into two steps: dynamic ramp-up of
 473 the contact force and static hold (Static hold procedure is
 474 not included in FAI validation since it only responds to
 475 onset and offset of the stimulation).

476 The benchmark model ‘TouchSim’ [8] for predicting the
 477 cutaneous neural response was employed to compare with
 478 the performance of this multi-level numerical model. Only

479 passive stimuli could be simulated by using ‘TouchSim’.
480 Therefore, the in-vivo discrimination test based on passive
481 stimuli was also conducted under the instruction of [41].
482 The discrimination accuracy achieved by ‘TouchSim’ was
483 then compared with the multi-level numerical model
484 together with the in-vivo experimental results in this study.
485 To configure the external stimuli in TouchSim [8], the
486 large rounded probs with the same diameters of the convex
487 surfaces used in our research were set as the external
488 stimuli. The density of the cutaneous receptors remained
489 default, only the tactile units located at the index fingertip
490 (Zone ‘D2d’ in TouchSim) were involved in the simulation.
491 The population-level responses of the SAI and FAI tactile
492 units evoked under the passive stimuli were then computed
493 through ‘TouchSim’.

494 III. RESULTS

495 A. Predicted tactile signals of the single afferent neural 496 fiber

497 The stress/strain related quantities including maximum
498 principal strain/stress, vertical strain etc. were correlated
499 with the results of microneurography and the quantity
500 achieving the best fit with the experimental results was
501 selected to be the input of the membrane current
502 transduction model. The stimulation onto the fingertip
503 during microneurography was simulated by using the FE
504 hand model. The strain energy density and other
505 stress/strain related mechanical quantities were obtained
506 under the stimulating force of 2N for the receptive field of
507 SAI and FAI unit. The spatial profiles of strain energy
508 density, maximum principal stress/strain and vertical stress
509 were compared with the microneurography results in Fig.
510 S2. A linear relationship between the neural action
511 potential level and mechanical quantities was assumed in
512 the form of:

$$513 N_i = aS_i + b..... (14)$$

514 Where N_i is the neural activation potential level and S_i
515 stands for the simulated results. The constants a and b were
516 derived by maximizing the FSS (equation 10) between the
517 microneurography data and the predicted mechanical
518 quantities.

519 The FSS value of 1 means a perfect match between
520 predictions and experiment results. Predictions were made
521 based on twelve different stress/strain related quantities
522 (see Table. S1) and it was found that strain energy density
523 can provide the best fit with the FSS values of 0.92 and
524 0.69 for SAI and FAI unit, respectively. This conclusion is
525 in agreement with other researchers [22]. Therefore, the
526 strain energy density was used to correlate the skin
527 mechanics with neural activity for this research.

528 The original and optimized parameters of the
529 transduction and Izhikevich neural dynamic model were
530 presented in Table S2 and S3. Four and six iterations of
531 RSM were performed for SAI and FAI unit respectively,
532 resulting in the FSS values of 0.9377 and 0.8235.

533 The neural action potential level under the stimulating
534 force of 2.4N for SAI and FAI unit are used as
535 out-of-sample validation (see Fig. 6). The predicted and
536 experimental spiking rates are close to each other for both

537 SAI and FAI units. For the SAI unit, the predicted results
538 got a wider range of variation than the experimental results.
539 The FAI unit only responded to the ‘onset’ and ‘offset’ of
540 the stimulation during the microneurography test while for
541 the predicted results, the FAI unit still fired a few spikes at
542 the lower frequencies.

543 B. Predicted tactile signals of the population-level 544 afferent neural fiber and its validation

545 The predicted spiking rates and first spike latency in
546 terms of the population-level afferent tactile units over the
547 finger pad were plotted and visualized in Figure 7. The
548 comparison between the predicted discrimination accuracy
549 and the *in-vivo* psychophysical experimental results is
550 presented in Figure 8 and 9. The active touch is divided
551 into two stages including the dynamic ramp-up of the
552 contact force and static hold of the finger.

553 It can be seen from Figure 8, the predicted
554 discrimination accuracy agreed well with the experimental
555 results. the convex with the curvature of RC8503, RC532,
556 RC179, RC106, RC77.7, RC48.9mm were numbered from
557 convex 1 to 6. The hit rates are all increased with the
558 curvature of the convex surfaces with regard to the first
559 spike latency and the two stages of the active touch. In the
560 case of the SAI unit, the predicted accuracies are larger
561 than those of the human subject for discriminating the
562 smaller curvatures (convex surface of RC8503, RC532mm
563 differentiated from the flat plate). Whereas the curvature
564 increases, the predicted accuracies are lower than the
565 subject’s (hit rate was close to 100%) for the convex
566 surface of RC77.7 and RC48.9mm. The predicted accuracy
567 during the static hold is closer to experimental results than
568 those in terms of the first spike latency and dynamic
569 ramp-up. The standard deviations for the predicted and
570 experimental results decrease with the curvature of the
571 convex.

572 Figure 9 shows the predictive accuracy and experimental
573 results for the FAI unit. The static hold is not included
574 since the FAI unit mainly responds to the dynamic
575 stimulation. In contrast to the SAI unit, the most accurate
576 prediction was achieved based on the first spike latency.
577 For the procedure of ‘Dynamic ramp-up’, the predicted
578 accuracies for discriminating convex surface with a small
579 radius are larger than the experimental results, while in the
580 case of discriminating convex surface with a larger radius
581 the predicted accuracies were smaller than the
582 experimental results. This is similar to the SAI unit. The
583 standard deviations for predicted and experimental results
584 are all decreased with the radius of the stimulator. The
585 discrimination accuracy predicted based on the uniformly
586 distributed receptive field of cutaneous neurons was
587 compared with that of heterogeneous one (See Fig. S3 and
588 S4). The results suggested that most of the discrimination
589 accuracy computed based on the tactile units with
590 heterogeneous receptive fields achieved a better agreement
591 with the human subject than the predicted results based on
592 the uniformly distributed receptive fields.

593 The discrimination accuracy achieved based on the
594 predicted afferent tactile signals through ‘TouchSim’ [8]
595 was compared with that using the multi-level numerical

596 model (See Fig. S5 and S6). The results showed that the
597 predicted neural signals through ‘TouchSim’ are consistent
598 with those based on the multi-level numerical model while
599 the predicted discrimination accuracy of ‘TouchSim’ is
600 slightly closer to the human subject than that of the
601 multi-level numerical model. However, these afferent
602 tactile signals were computed under the condition of
603 passive stimuli, the skin mechanics under active touch is
604 not accessible through ‘TouchSim’ [8]. Therefore, the
605 multi-level model developed in this research achieved
606 comparable performance with ‘TouchSim’ on predicting
607 the afferent tactile signals under passive stimuli but with a
608 further capability to obtain the cutaneous neural response
609 evoked during active touch.

610 IV. DISCUSSION

611 In this study an integrated numerical model was
612 developed and validated for SAI and FAI afferent,
613 combining the skin mechanics and neural dynamics to
614 predict the single and population-level response of the 1st
615 order cutaneous neurons. The model development was
616 carried out on three levels: (A) on the skin mechanics level
617 by using a subject-specific FE human hand model, (B)
618 validation of the signals from single afferent fiber with the
619 FSS of 0.94 and 0.82 for SAI and FAI unit respectively
620 compared to the microneurography results, (C) the
621 discrimination accuracies of two tactile units achieved the
622 good agreement with the *in-vivo* discrimination test results.
623 The model of population-level neural tactile SAI and FAI
624 unit can differentiate the convex surface with RC8503mm
625 from a flat plate.

626 The FE human hand served as the skin mechanics model
627 so that the muscle forces and kinematics of active touch can
628 be incorporated. The transduction mechanism between the
629 afferent neural signal and neural activation level of the
630 muscle synergy during active touch can also be
631 investigated. Therefore, this integrated numerical model
632 provides the possibility and push a further step to the
633 explicit studying of sensorimotor mechanism compared
634 with previous studies [9, 22, 45]. The realistic contact
635 mechanism and anatomically intact human hand model
636 provide the actual skin mechanics for predicting neural
637 signals, rather than using the simplified continuum model
638 or regression algorithm [8, 41, 46]. Also, this integrated
639 model can help to predict reliable afferent cutaneous neural
640 signals without the need to carry out microneurography or
641 microsimulation as done previously [15-17, 47]. The
642 subject-specific microneurography and *in-vivo*
643 psychophysical experimental data with an integrated
644 numerical model were employed to study the tactile neural
645 coding and human perception. The predicted
646 population-level 1st order neural signals under active tactile
647 exploration suggest that different coding mechanisms
648 might be applied for the afferent tactile signals elicited
649 from different mechanoreceptors simultaneously.

650 Microneurography was performed on the subject of the
651 FE hand model. Approximately 75% of the test results
652 were applied for the optimization of the transduction and
653 Izhikevich neural dynamic model, the other 25% of data

654 was used for validation against the predicted results. For
655 the validation of an SAI tactile unit the predicted firing
656 rates varied more greatly than the experimental results, this
657 may be due to the hyperplastic material properties defined
658 for soft tissues in the FE model. The stress is sensitive to
659 the strain variation resulting in large variations of SED and
660 membrane current. In the case of the FAI unit, the predicted
661 firing rates agreed well with the microneurography results
662 during the ‘onset’ and ‘offset’, achieving the FSS of 0.82
663 for all the data points. However, when the RTS was
664 sweeping over the receptive area of the FAI unit, the
665 receptors gave no response with the neural action potential
666 level of 0 spikes/second while the predicted spiking rate
667 was maintained at approximately 20 spikes/second. It can
668 be found from the neural dynamic model for the FAI unit
669 (see equation 4), the firing rate depends on the derivative of
670 the membrane current on the time domain. The SED varied
671 slightly when the stimulator was sweeping over FE hand
672 while this variation may initiate the drifting of the
673 predicted membrane current.

674 The probabilistic psychophysical prediction was made
675 by using the Gradient Sum method. The spiking rate or the
676 first spike latency was transferred element by element
677 throughout the population. Therefore, each convexity can
678 be represented as a single number as the gradient sum. Here,
679 the population responses during active touch were obtained
680 and compared with the subject-specific discrimination
681 results. The predicted discrimination results for both SAI
682 and FAI units agreed well with the experimental results.
683 During the *in-vivo* discrimination test, the convex surfaces
684 with a small curvature like RC48.9mm is easy to be
685 discriminated from flat plate for the human subject (from
686 the subject’s personal feeling). Therefore, the experimental
687 discrimination accuracies of population-level SAI and FAI
688 units are smaller than the predicted ones for discriminating
689 convex surfaces with small curvatures while in case of
690 discriminating the convex surface with a large radius, the
691 subject’s success rate became smaller than the simulated
692 results. This might be affected by the subject’s human
693 factor since a large number of comparisons need to be
694 completed through the experiment. The two stages of
695 active touch and the first spike latency are good candidates
696 to make the prediction based on this multi-physics model.
697 However, the static hold can provide the best fit for the
698 human discrimination test results which means the
699 perception may rely on rate coding for the signals from SAI
700 units. Unlike the SAI units, perception may depend on the
701 temporal coding of FAI afferents since the predicted
702 accuracy based on first spike latency achieved the best
703 agreement with the experimental results. These findings
704 support the assumptions made by other researchers [48, 49]
705 that humans may use multiple coding strategies
706 simultaneously. The temporal coding may be used for fast
707 identification of a stimulus and triggering the reactions
708 while rate coding can represent the quantities of the
709 stimulus. The similar perception was evoked based on the
710 neural information conveyed by these two tactile afferents
711 but relying on two different coding mechanisms,
712 suggesting that different types of tactile neurons could be
713 independent in haptic systems. The noise applied to the

714 firing rates and first spike latency can affect the predicted
715 accuracy, the effect was shown in Fig. S7. The simulation
716 results have shown that the complex and heterogeneous
717 distributed receptive field of cutaneous neurons help to
718 enhance the discrimination accuracy compared with those
719 under the uniform distribution. These larger and more
720 complex overlapped receptive fields with multiple ‘hotspots’
721 or sensitive zones enable a higher spatial resolution which
722 echoes the finding of other researchers [25]. However, the
723 afferent branching mechanism through which the end
724 organs of the cutaneous receptors are integrated to elicit the
725 afferent neural signals is still unclear so far [29, 50]. More
726 simulations on active touch could be conducted to study the
727 effects of these heterogeneous receptive fields on human
728 tactile performance after gaining a solid understanding of
729 the branching mechanism of cutaneous receptors.

730 The discrimination accuracy archived based on the
731 cutaneous neural responses predicted through this
732 multi-level model was compared with that of ‘TouchSim’
733 [8]. ‘TouchSim’ achieved a more human-like tactile
734 performance than the multi-level numerical model based
735 on the passive external stimuli. Despite the high computing
736 efficiency and better performance of ‘TouchSim’ under
737 passive stimuli [8], the multilevel numerical model
738 developed in this study takes the 3D geometry of the
739 human hand and the muscle-driven active touch into
740 consideration while maintaining a comparable
741 performance on predicting the afferent tactile signals with
742 ‘TouchSim’.

743 This validated multi-level numerical model provides the
744 possibility for pioneering research on human tactile
745 sensing under the active touch and sensorimotor
746 mechanism. For example, the relationship between
747 population-level afferent signals and the neural activation
748 level of muscle synergy could be explicitly summarized
749 and applied to the control of bionic or prosthetic hand to
750 restore the performance of the human hand [51, 52].
751 However, the FE human hand model was involved in this
752 numerical tool, resulting in the high computational cost.
753 The surrogate modelling based on this FE model needs to
754 be developed to reduce the computational cost and make it
755 user-friendly to other researchers. Also, this multi-level
756 numerical model can only predict the neural response of
757 two type I tactile units. The convergence of the 1st order
758 tactile signals from the ulna and median nerve and their
759 post-processing were not included in this research. Future
760 work can focus on simulating the responses of the two type
761 II mechanoreceptors and the convergent mechanism of the
762 population-level cutaneous neural signals transferred along
763 different nerves.

764 V. CONCLUSION

765 The FE human hand model was combined with
766 mechano-electrical transduction and neural dynamic model
767 for predicting afferent tactile neural signals during active
768 tactile exploration. The relationship between external
769 stimuli and cutaneous neural activities was computed
770 based on subject-specific microneurography data,
771 approximately 75% of the test results was applied for the

772 model optimization and another 25% was used for
773 validation. Human perception during an active
774 discriminating test was correlated with the population-level
775 tactile neural signals achieving similar tactile
776 discrimination abilities to the human subject. The predicted
777 cutaneous neural signals under active touch suggest that
778 human perception during active touch exploration may
779 simultaneously rely on different coding mechanisms for
780 the neural signals elicited from different classes of
781 cutaneous receptors. It was found that the heterogeneously
782 distributed receptive fields may help to achieve a better
783 sensing performance than the uniformly distributed ones.
784 Comparable discrimination accuracies are observed
785 between this multi-level numerical model and the
786 published benchmark model [8], while the former presents
787 the further capability of predicting the afferent neural
788 response under the active touch. The 3D geometry of the
789 finger pad and hand kinematics are also involved. This
790 integrated numerical model provides a new concept to
791 effectively study the human tactile seeing and sensorimotor
792 mechanism under the active touch.

793 ACKNOWLEDGEMENT

795 This research was partly supported by the National Key
796 Research and Development Program of China (grant
797 2018YFC2001300), the National Natural Science
798 Foundation of China (grants 91948302, 91848204, and
799 52021003).

801 CONFLICT OF INTEREST

802 The authors declare that they have no conflicts of
803 interest.

804 REFERENCES

- 805 [1] E. R. Kandel *et al.*, *Principles of neural science*.
806 McGraw-hill New York, 2000.
- 807 [2] G. Valle *et al.*, "Biomimetic Intraneural Sensory
808 Feedback Enhances Sensation Naturalness,
809 Tactile Sensitivity, and Manual Dexterity in a
810 Bidirectional Prosthesis," *Neuron*, vol. 100, no. 1,
811 pp. 37-45 e7, Oct 10 2018, doi:
812 10.1016/j.neuron.2018.08.033.
- 813 [3] K. O. Johnson, "Neural coding," *Neuron*, vol. 26,
814 no. 3, pp. 563-566, 2000.
- 815 [4] B. M. Calancie and R. Stein, "Microneurography
816 for the recording and selective stimulation of
817 afferents: An assessment," *Muscle & Nerve:
818 Official Journal of the American Association of
819 Electrodiagnostic Medicine*, vol. 11, no. 6, pp.
820 638-644, 1988.
- 821 [5] A. B. Vallbo, K.-E. Hagbarth, and B. G. Wallin,
822 "Microneurography: how the technique
823 developed and its role in the investigation of the
824 sympathetic nervous system," *Journal of Applied
825 Physiology*, vol. 96, no. 4, pp. 1262-1269, 2004.
- 826 [6] K. Dandekar, B. I. Raju, and M. A. Srinivasan,
827 "3-D finite-element models of human and monkey

- 828 fingertips to investigate the mechanics of tactile
829 sense," *Journal of biomechanical engineering*,
830 vol. 125, no. 5, pp. 682-691, 2003.
- 831 [7] G. J. Gerling, Rivest, II, D. R. Lesniak, J. R.
832 Scanlon, and L. Wan, "Validating a population
833 model of tactile mechanotransduction of slowly
834 adapting type I afferents at levels of skin
835 mechanics, single-unit response and
836 psychophysics," *IEEE Trans Haptics*, vol. 7, no. 2,
837 pp. 216-28, Apr-Jun 2014, doi:
838 10.1109/TOH.2013.36.
- 839 [8] H. P. Saal, B. P. Delhaye, B. C. Rayhaun, and S. J.
840 Bensmaia, "Simulating tactile signals from the
841 whole hand with millisecond precision,"
842 *Proceedings of the National Academy of Sciences*,
843 vol. 114, no. 28, pp. E5693-E5702, 2017.
- 844 [9] D. R. Lesniak and G. J. Gerling, "Predicting SA-I
845 mechanoreceptor spike times with a skin-neuron
846 model," *Math Biosci*, vol. 220, no. 1, pp. 15-23,
847 Jul 2009, doi: 10.1016/j.mbs.2009.03.007.
- 848 [10] C. Xu, Y. Wang, and G. J. Gerling, "Individual
849 Performance in Compliance Discrimination is
850 Constrained by Skin Mechanics but Improved
851 under Active Control," in *2021 IEEE World
852 Haptics Conference (WHC)*, 2021: IEEE, pp.
853 445-450.
- 854 [11] C. Simões-Franklin, T. A. Whitaker, and F. N.
855 Newell, "Active and passive touch differentially
856 activate somatosensory cortex in texture
857 perception," *Human brain mapping*, vol. 32, no. 7,
858 pp. 1067-1080, 2011.
- 859 [12] A. M. Smith, C. E. Chapman, F. Donati, P.
860 Fortier-Poisson, and V. Hayward, "Perception of
861 simulated local shapes using active and passive
862 touch," *Journal of neurophysiology*, vol. 102, no.
863 6, pp. 3519-3529, 2009.
- 864 [13] R. Grant, P. M. Itskov, B. Towal, and T. J.
865 Prescott, "Active touch sensing: finger tips,
866 whiskers, and antennae," *Frontiers in behavioral
867 neuroscience*, vol. 8, p. 50, 2014.
- 868 [14] R. S. Johansson and J. R. Flanagan, "Coding and
869 use of tactile signals from the fingertips in object
870 manipulation tasks," *Nature Reviews
871 Neuroscience*, vol. 10, no. 5, pp. 345-359, 2009.
- 872 [15] J. Ochoa and E. Torebjörk, "Sensations evoked by
873 intraneural microstimulation of single
874 mechanoreceptor units innervating the human
875 hand," *The Journal of physiology*, vol. 342, no. 1,
876 pp. 633-654, 1983.
- 877 [16] R. Romo, "Hernandez A, Zainos A, and Salinas
878 E," *Somatosensory discrimination based on
879 cortical microstimulation. Nature*, vol. 392, pp.
880 387-390, 1998.
- 881 [17] S. N. Flesher *et al.*, "Intracortical
882 microstimulation of human somatosensory
883 cortex," *Science translational medicine*, vol. 8, no.
884 361, pp. 361ra141-361ra141, 2016.
- 885 [18] B. Lee *et al.*, "Engineering artificial
886 somatosensation through cortical stimulation in
887 humans," *Frontiers in systems neuroscience*, vol.
888 12, p. 24, 2018.
- 889 [19] Y. Wei, Z. Zou, G. Wei, L. Ren, and Z. Qian,
890 "Subject-specific finite element modelling of the
891 human hand complex: muscle-driven simulations
892 and experimental validation," *Annals of
893 Biomedical Engineering*, pp. 1-15, 2019.
- 894 [20] G. Harih, R. Nohara, and M. Tada, "Finite
895 Element Digital Human Hand Model-Case Study
896 of Grasping a Cylindrical Handle," *Journal of
897 Ergonomics*, vol. 07, no. 02, 2017, doi:
898 10.4172/2165-7556.1000190.
- 899 [21] J. R. Holt and D. P. Corey, "Two mechanisms for
900 transducer adaptation in vertebrate hair cells,"
901 *Proceedings of the National Academy of Sciences*,
902 vol. 97, no. 22, pp. 11730-11735, 2000.
- 903 [22] T. Q. Pham, T. Hoshi, Y. Tanaka, and A. Sano,
904 "Effect of 3D microstructure of dermal papillae
905 on SED concentration at a mechanoreceptor
906 location," *PloS one*, vol. 12, no. 12, p. e0189293,
907 2017.
- 908 [23] J. A. Pruszynski and R. S. Johansson,
909 "Edge-orientation processing in first-order tactile
910 neurons," *Nature neuroscience*, vol. 17, no. 10, pp.
911 1404-1409, 2014.
- 912 [24] R. S. Johansson, "Tactile sensibility in the human
913 hand: receptive field characteristics of
914 mechanoreceptive units in the glabrous skin area,"
915 *The Journal of physiology*, vol. 281, no. 1, pp.
916 101-125, 1978.
- 917 [25] E. Jarocka, J. A. Pruszynski, and R. S. Johansson,
918 "Human touch receptors are sensitive to spatial
919 details on the scale of single fingerprint ridges,"
920 *Journal of Neuroscience*, vol. 41, no. 16, pp.
921 3622-3634, 2021.
- 922 [26] N. Cauna, "Nerve supply and nerve endings in
923 Meissner's corpuscles," *American Journal of
924 Anatomy*, vol. 99, no. 2, pp. 315-350, 1956.
- 925 [27] N. Cauna, "The mode of termination of the
926 sensory nerves and its significance," *Journal of
927 Comparative Neurology*, vol. 113, no. 2, pp.
928 169-209, 1959.
- 929 [28] M. Nolano *et al.*, "Quantification of myelinated
930 endings and mechanoreceptors in human digital
931 skin," *Annals of neurology*, vol. 54, no. 2, pp.
932 197-205, 2003.
- 933 [29] M. Paré, A. M. Smith, and F. L. Rice,
934 "Distribution and terminal arborizations of
935 cutaneous mechanoreceptors in the glabrous
936 finger pads of the monkey," *Journal of
937 Comparative Neurology*, vol. 445, no. 4, pp.
938 347-359, 2002.
- 939 [30] R. S. Johansson and A. B. Vallbo, "Tactile
940 sensibility in the human hand: relative and
941 absolute densities of four types of
942 mechanoreceptive units in glabrous skin," *The
943 Journal of physiology*, vol. 286, no. 1, pp.
944 283-300, 1979.

- 945 [31] D. Quintero, "Properties of cutaneous
946 mechanoreceptors in the human hand-related to
947 touch sensation," 1984.
- 948 [32] E. M. Izhikevich, "Simple model of spiking
949 neurons," *IEEE Transactions on neural networks*,
950 vol. 14, no. 6, pp. 1569-1572, 2003.
- 951 [33] A. Chami, M. Ohka, Y. Kawabe, and H. B.
952 Yussof, "Response of SAI Afferents May Play a
953 Role in the Perception of Velvet Hand Illusion 1,"
954 2010.
- 955 [34] M. Condon *et al.*, "Differential sensitivity to
956 surface compliance by tactile afferents in the
957 human finger pad," *Journal of Neurophysiology*,
958 vol. 111, no. 6, pp. 1308-1317, 2014.
- 959 [35] S. B. Park *et al.*, "Fast-adapting mechanoreceptors
960 are important for force control in precision grip
961 but not for sensorimotor memory," *Journal of*
962 *neurophysiology*, vol. 115, no. 6, pp. 3156-3161,
963 2016.
- 964 [36] R. S. Johansson and Å. B. Vallbo, "Tactile
965 sensory coding in the glabrous skin of the human
966 hand," *Trends in neurosciences*, vol. 6, pp. 27-32,
967 1983.
- 968 [37] R. G. Hallin, "Microneurography in relation to
969 intraneural topography: somatotopic organisation
970 of median nerve fascicles in humans," *Journal of*
971 *Neurology, Neurosurgery & Psychiatry*, vol. 53,
972 no. 9, pp. 736-744, 1990.
- 973 [38] N. D. Strzalkowski, R. M. Peters, J. T. Inglis, and
974 L. R. Bent, "Cutaneous afferent innervation of the
975 human foot sole: what can we learn from
976 single-unit recordings?," *Journal of*
977 *neurophysiology*, vol. 120, no. 3, pp. 1233-1246,
978 2018.
- 979 [39] N. Salimi-Nezhad, M. Amiri, E. Falotico, and C.
980 Laschi, "A Digital Hardware Realization for
981 Spiking Model of Cutaneous Mechanoreceptor,"
982 *Frontiers in Neuroscience*, vol. 12, 2018.
- 983 [40] H. Stanislaw and N. Todorov, "Calculation of
984 signal detection theory measures," *Behavior*
985 *research methods, instruments, & computers*, vol.
986 31, no. 1, pp. 137-149, 1999.
- 987 [41] A. Goodwin, K. John, and A. Marceglia, "Tactile
988 discrimination of curvature by humans using only
989 cutaneous information from the fingerpads,"
990 *Experimental brain research*, vol. 86, no. 3, pp.
991 663-672, 1991.
- 992 [42] F. D. Farfan, J. C. Politti, and C. J. Felice,
993 "Evaluation of EMG processing techniques using
994 Information Theory," *Biomed Eng Online*, vol. 9,
995 p. 72, Nov 12 2010, doi:
996 10.1186/1475-925X-9-72.
- 997 [43] C. J. De Luca, L. D. Gilmore, M. Kuznetsov, and
998 S. H. Roy, "Filtering the surface EMG signal:
999 Movement artifact and baseline noise
1000 contamination," *J Biomech*, vol. 43, no. 8, pp.
1001 1573-9, May 28 2010, doi:
1002 10.1016/j.jbiomech.2010.01.027.
- 1003 [44] T. Butler, S. Kilbreath, R. Gorman, and S.
1004 Gandevia, "Selective recruitment of single motor
1005 units in human flexor digitorum superficialis
1006 muscle during flexion of individual fingers," *The*
1007 *Journal of physiology*, vol. 567, no. 1, pp.
1008 301-309, 2005.
- 1009 [45] F. Crevecoeur, A. Barrea, X. Libouton, J. L.
1010 Thonnard, and P. Lefevre, "Multisensory
1011 components of rapid motor responses to fingertip
1012 loading," *J Neurophysiol*, vol. 118, no. 1, pp.
1013 331-343, Jul 1 2017, doi: 10.1152/jn.00091.2017.
- 1014 [46] R. S. Johansson and I. Birznieks, "First spikes in
1015 ensembles of human tactile afferents code
1016 complex spatial fingertip events," *Nature*
1017 *neuroscience*, vol. 7, no. 2, p. 170, 2004.
- 1018 [47] L. Johnson, J. Wander, D. Sarma, D. Su, E. Fetz,
1019 and J. Ojemann, "Direct electrical stimulation of
1020 the somatosensory cortex in humans using
1021 electrocorticography electrodes: a qualitative and
1022 quantitative report," *Journal of Neural*
1023 *Engineering*, vol. 10, no. 3, p. 036021, 2013.
- 1024 [48] M. Bieler, K. Sieben, N. Cichon, S. Schildt, B.
1025 Röder, and I. L. Hanganu-Opatz, "Rate and
1026 temporal coding convey multisensory information
1027 in primary sensory cortices," *eneuro*, vol. 4, no. 2,
1028 2017.
- 1029 [49] S. Terada, Y. Sakurai, H. Nakahara, and S.
1030 Fujisawa, "Temporal and rate coding for discrete
1031 event sequences in the hippocampus," *Neuron*,
1032 vol. 94, no. 6, pp. 1248-1262. e4, 2017.
- 1033 [50] E. D. Kuehn, S. Meltzer, V. E. Abraira, C.-Y. Ho,
1034 and D. D. Ginty, "Tiling and somatotopic
1035 alignment of mammalian low-threshold
1036 mechanoreceptors," *Proceedings of the National*
1037 *Academy of Sciences*, vol. 116, no. 19, pp.
1038 9168-9177, 2019.
- 1039 [51] Y. Kim *et al.*, "A bioinspired flexible organic
1040 artificial afferent nerve," *Science*, vol. 360, no.
1041 6392, pp. 998-1003, 2018.
- 1042 [52] J. J. Cone, A. M. Ni, K. Ghose, and J. H. Maunsell,
1043 "Electrical microstimulation of visual cerebral
1044 cortex elevates psychophysical detection
1045 thresholds," *Eneuro*, vol. 5, no. 5, 2018.

1046